Geophysical Journal International

Geophys. J. Int. (2014) **196,** 15–21
Advance Access publication 2013 October 29

doi: 10.1093/gji/ggt379

The 2012 August 11 Ahar earthquakes: consequences for tectonics and earthquake hazard in the Turkish–Iranian Plateau

Alex Copley,[1] Mohammad Faridi,[2] Manoucher Ghorashi,[3] James Hollingsworth,[4] James Jackson,[1] Hamid Nazari,[3] Behnam Oveisi[5] and Morteza Talebian[3]

[1]*COMET+, Bullard Labs, Department of Earth Sciences, University of Cambridge, Cambridge, United Kingdom. E-mail: acc41@cam.ac.uk*
[2]*Geological Survey of Iran, Northwestern Regional Office, Tabriz, Iran*
[3]*Research Institute for Earth Sciences, Geological Survey of Iran, Azadi Square, Meraj Blvd, Tehran, Iran*
[4]*CNRS, Geoazur, Universite Nice Sophia Antipolis, Nice, France*
[5]*Seismotectonics Department, Geological Survey of Iran, Azadi Square, Meraj Blvd, Tehran, Iran*

Accepted 2013 September 17. Received 2013 September 17; in original form 2013 June 18

SUMMARY

We have examined the faulting in the 2012 August 11 M_w 6.4 and 6.3 Ahar (NW Iran) earthquakes using a combination of field mapping, remote-sensing observations of tectonic geomorphology, the cross-correlation of optical satellite images and the inversion of seismic waveforms. The first event was close to pure strike-slip, and the second was an oblique combination of thrust and strike-slip motion. Mapped surface ruptures indicate at least one of these events accommodated mostly right-lateral strike-slip motion on an ∼E–W striking plane. The occurrence of these earthquakes highlights the spatially distributed deformation in NW Iran, which has implications for both hazard assessment (the Ahar events killed over 300 people and injured over 3000), and also tectonic models of the region. Furthermore, these earthquakes demonstrate that the tectonics of the Ahar area is characterized by strike-slip faulting and a component of shortening, and not the previously suggested extension.

Key words: Earthquake source observations; Continental neotectonics; Asia.

1 INTRODUCTION

On 2012 August 11 two destructive earthquakes occurred 11 min apart near the town of Ahar in NW Iran (M_w 6.4 at 12:23 UTC and M_w 6.3 at 12:34 UTC; Figs 1 and 2), resulting in over 300 deaths and 3000 injuries. The wider tectonics of the Arabia–Eurasia collision zone at the longitude of NW Iran and E Turkey is characterized by right-lateral strike-slip faulting on WNW–ESE planes in the Turkish–Iranian Plateau, and thrust faulting with the same strike in the Greater Caucasus further north (Fig. 1a). This arrangement of faulting accommodates the oblique northwestward convergence of Arabia with Eurasia by the spatial separation (partitioning) of the faults accommodating the strike-slip and shortening components of motion (Jackson 1992; McClusky *et al.* 2000; Copley & Jackson 2006). The partitioning of thrust and strike-slip faulting in this way can also clearly be seen in the Global Positioning System (GPS) velocities shown in Fig. 1(b) (Masson *et al.* 2006; Reilinger *et al.* 2006; Djamour *et al.* 2011). Strike-slip faulting within the Turkish–Iranian Plateau accommodates the change in motion relative to Eurasia from NNW in the south near Lake Urumiyeh (LU in Fig. 1b) to NE in the northern part of the plateau. The decrease in velocities within the Greater Caucasus results from thrust faulting on the southern margin of the range. The Ahar earthquakes are within the zone of right-lateral strike-slip faulting in the Turkish–Iranian Plateau that accommodates the strike-slip component of the overall Arabia–Eurasia relative motion (Fig. 1).

The Ahar earthquakes occurred on previously unrecognized active faults, north of the well-known North Tabriz Fault (e.g. Ambraseys & Melville 1982; Hessami *et al.* 2003, NTF in Fig. 1a). They provide an opportunity to improve our knowledge of both the distribution of active faults in the region and of the seismic hazard faced by local populations. The earthquakes additionally provide a new insight into the active tectonics of NW Iran and the Turkish–Iranian Plateau as a whole.

We first describe the faulting that occurred during the two earthquakes, using a combination of field observations, optical satellite geodesy and the inversion of *P* and *SH* seismic waveforms. We then discuss the tectonics of NW Iran and the surrounding regions in light of our results, and finally summarize the implications of these earthquakes for tectonic models of continental regions and the assessment of seismic hazard.

2 FIELD OBSERVATIONS AND GEOMORPHOLOGY

Fig. 2(a) shows the topography in the epicentral region of the earthquakes, and the locations of mapped surface ruptures. The observed

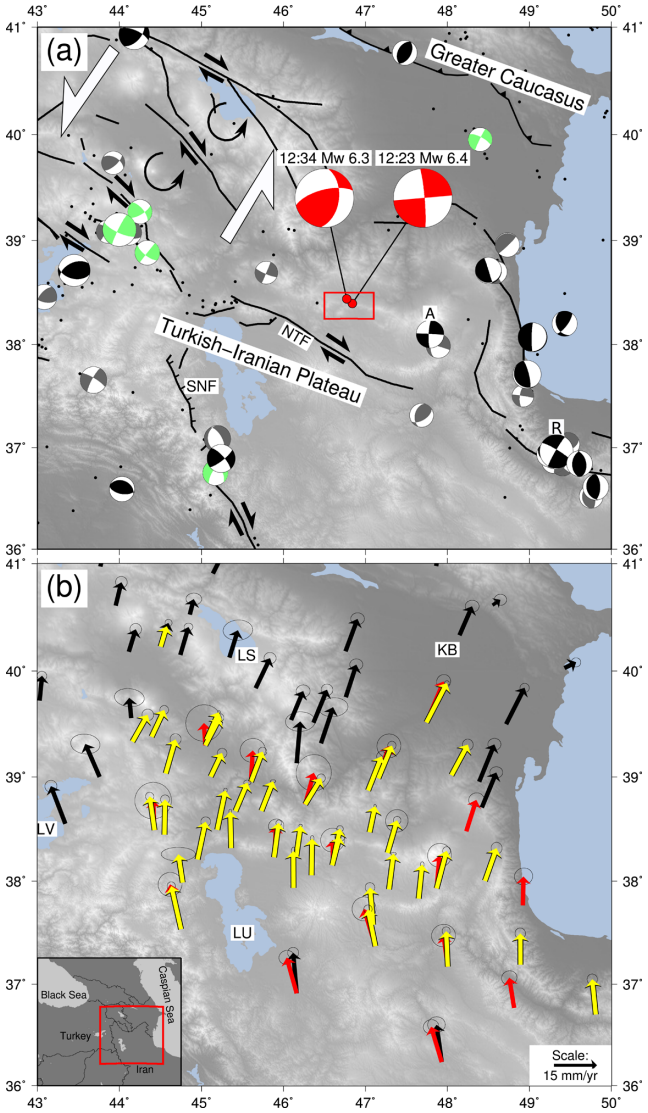

Figure 1. (a) Earthquakes in the Turkish–Iranian Plateau [inset to (b) shows area of coverage and national borders]. Black dots are earthquakes in the EHB catalogue (Engdahl *et al.* 1998), green focal mechanisms are from first motions, grey are global CMT solutions (www.globalcmt.org) and black are from modelling of *P* and *SH* waveforms [from Elliott *et al.* (2013) and the compilation of Copley & Jackson (2006)]. We show only earthquakes with depths reported as less than 50 km, which excludes some deep events from the Apsheron–Balkhan sill in the central Caspian (Jackson *et al.* 2002), and some isolated deep events beneath the Kura Basin [KB on (b); Mellors *et al.* 2012], which are thought to be related to active or recent subduction. The two red focal mechanisms represent the 2012 Ahar events. The 12:23 mechanism is from our waveform modelling, and the 12:34 mechanism is the global CMT solution. 'A' shows the 1997 M_w 6.0 Ardebil earthquake, 'R' shows the 1990 M_w 7.3 Rudbar earthquake, NTF shows the North Tabriz Fault and SNF represents the Serow normal faults. Mapped faults are from Jackson *et al.* (2002) and Copley & Jackson (2006). Large white arrows show the overall right-lateral shear on NE/SW planes in the northern Turkish–Iranian Plateau, which is accommodated by anticlockwise rotations (black-curved arrows) and right-lateral strike-slip faulting (Copley & Jackson 2006). The red box shows the area of coverage of Fig. 2. (b) GPS velocities relative to Eurasia from Reilinger *et al.* (2006; black), Masson *et al.* (2006; red) and Djamour *et al.* (2011; yellow). LU, LV and LS represent lakes Urumiyeh, Van and Sevan. KB shows the Kura Basin.

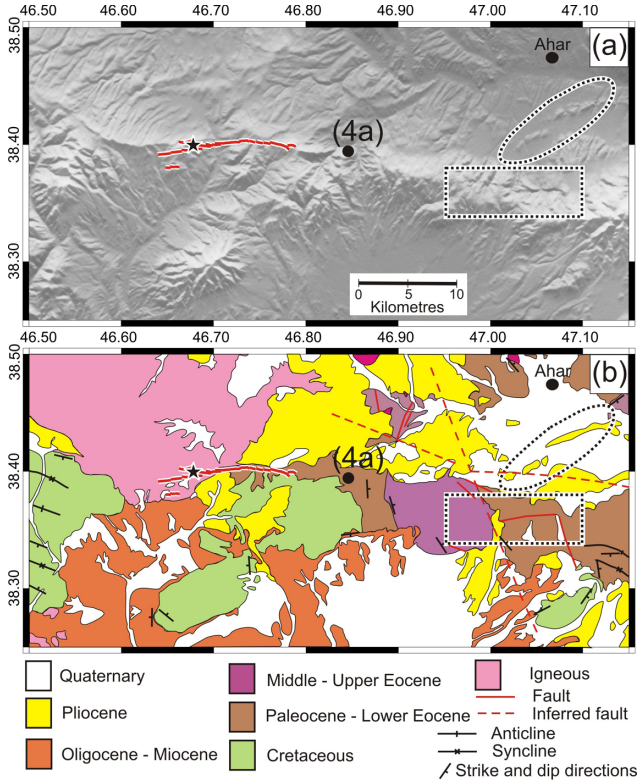

Figure 2. (a) Topography in the region shown by the red box in Fig. 1(a), illuminated from the north. Mapped surface ruptures are 13 km long and shown by red lines. The black star shows the location of the photographs in Fig. 3. The dotted black oval in the east shows NE–SW trending topographic ridges, as discussed in the text. The dotted rectangle outlines an E–W lineation running through the topography. (b) Simplified geological map, adapted from Geological Survey of Iran (1978). The location of Fig. 4(a) is marked on the figures.

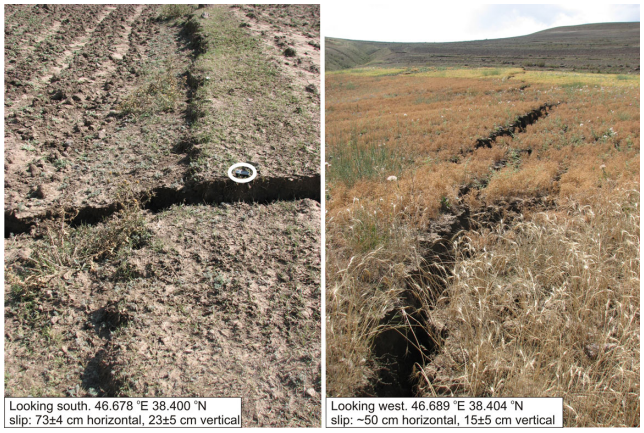

Figure 3. Surface ruptures photographed at the location shown by the black star on Fig. 2(a). (a) Right-lateral offset of a field boundary, with the scale given by a hand-held GPS receiver (circled). (b) Left-stepping en echelon fissures viewed along-strike. Photos by Behnam Oveisi.

surface faulting was dominantly right-lateral strike-slip of up to about 1 m (Fig. 3a), with minor up-to-the-south vertical motion. The ruptures were left-stepping en echelon fissures on scales of metres to tens of metres long (Fig. 3b), and stretch for ~13 km, occurring near the crests of two broad topographic ridges and crossing an

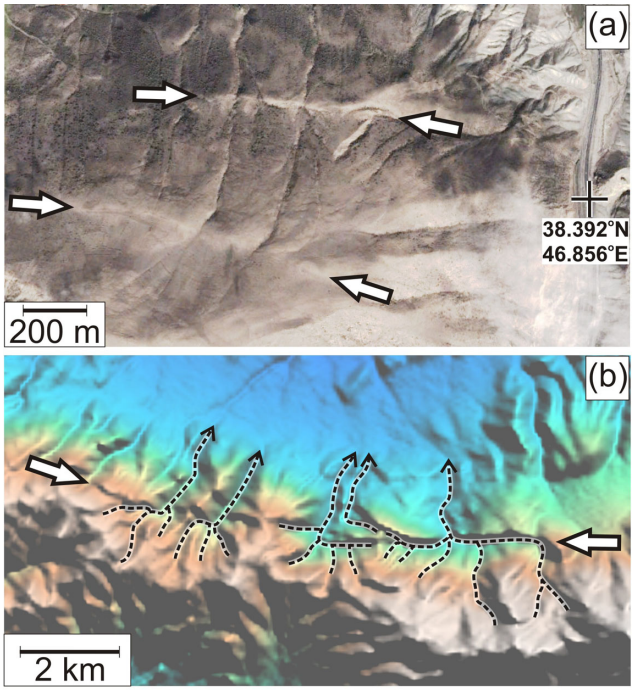

Figure 4. (a) WorldView image of the location marked '4a' on Fig. 2. Faults inferred in the landscape are marked by arrows. Image from Google Earth (copyright Google 2013 and Digital Globe 2013). (b) Topography (illuminated from the north) from the region of the dotted rectangle in Fig. 2. The white arrows show an inferred fault characterized by a prominent lineation in the topography, that in many places reverses the regional slope, and which diverts drainage (black-dashed lines) along it.

intervening valley (Fig. 2a). The ∼E–W orientation of the ruptures is consistent with formation during either of the two 2012 Ahar events if the ∼E–W nodal planes in the focal mechanisms (Fig. 1) are the fault planes.

Other faults can be inferred in the landscape, and Fig. 4(a) shows an example from along-strike of the earthquake rupture. However, the geomorphological expression of the faulting is discontinuous and for much of the length of the observed surface ruptures there is little clear indication of prior active faulting visible in the landscape. The location of the surface ruptures in 2012 near a ridge top may be responsible for the lack of distinctive tectonic geomorphology: there is no significant drainage that can be offset by the faulting, and ridge tops are likely to suffer relatively high erosion, especially during times of snowmelt.

Active faulting is suggested by the geomorphology beyond the eastern end of the 2012 surface ruptures. A clear E–W topographic lineation (black-dotted rectangle on Fig. 2a) strikes at a high angle to the local bedding and lithological boundaries (Geological Survey of Iran 1978, and Fig. 2b), and in places reverses the regional slope and disrupts the drainage patterns, so is likely to be produced by active faulting (Fig. 4b). NE–SW striking elongate ridges on the northern flank of the main mountain range in the area (black-dotted oval on Fig. 2a) are composed of Pliocene conglomerates rising above the surrounding Quaternary alluvium (Geological Survey of Iran 1978, and Fig. 2b) and show an offset in the regional slope across them, disrupting the local drainage, so are likely to be underlain by active blind thrusts. There are no reports of these structures having been active during the Ahar earthquakes, but they do suggest that other active faults are present in the region, along-strike of the fault that ruptured in 2012.

3 OPTICAL IMAGE CORRELATIONS

We have mapped the location of surface faulting, and the amount of slip, by cross-correlating WorldView optical satellite images using the COSI-Corr software (Leprince *et al.* 2007, 2008; Ayoub *et al.* 2009). When coregistering and reprojecting oblique WorldView images into a common viewing geometry prior to correlation, large non-tectonic signals can be generated by errors in the topographic data set used. To minimize this effect, we compute the displacement between the images in the plane perpendicular to the epipolar direction. The epipolar direction is the plane of maximum stereo parallax, so by computing the displacements in the plane perpendicular to this, we reduce the noise level relating to unmodelled topographic effects (Hollingsworth *et al.* 2012). Because the epipolar-perpendicular direction (azimuth 045°) is oblique to the E–W strike of the fault, our estimated fault displacement is only one component of the true motion. To constrain the full 2-D horizontal displacement field using this method, we would need additional pre- and post-earthquake WorldView images yielding an epipolar-perpendicular direction orthogonal to the first pair. As we lack suitable images, we extrapolate the NE–SW displacement field onto an E–W fault by assuming strike-slip motion (based on the field observations and focal mechanisms).

We used WorldView images acquired on 2010 December 24 and 2012 August 19 for the eastern part of the epicentral area (the earthquakes were on 2012 August 11), WorldView images from 2010 September 17 and 2012 August 19 for the western part of the region, and the ASTER GDEM version 2 topographic data set (30 m horizontal resolution). The results of the image correlations are shown in Fig. 5. This method is sensitive to displacement discontinuities, and not long wavelength signals. We image an E–W trending fault rupture ∼8 km long. The eastern part of the imaged slip (east of 46.7°E longitude) matches the location of the surface ruptures mapped in the field (Fig. 2a). West of this, the surface ruptures mapped in the field correspond to no clear signal in the WorldView image cross-correlation results, which may imply a decrease in surface slip towards that end of the rupture (to below the noise level in the data). The average fault offset estimated from the image correlations is $\sim 1.5 \pm 0.5$ m. There are three possible reasons why this value is slightly higher than observed in the field (<1 m, Fig. 3). The assumption of pure strike-slip motion could bias the optical correlation results to higher values than would be the case if a vertical component were also present. Alternatively, there are other well-documented examples of optical image correlations giving higher slip estimates than field observations (e.g. the Duzce earthquake, Konca *et al.* 2010), which are interpreted to mean some of the surface slip was accommodated as distributed deformation in the near-surface, in addition to the rupture on a discrete plane. Finally, the extrapolation up to the fault trace of the regional (non-tectonic) gradient in the cross-correlation results north of the fault (Fig. 5b) could have resulted in an overestimate of the offset on the fault. If the fault offset is taken to be represented by the single large step in the cross-correlation results, the estimated offset reduces to ∼1 m.

4 SEISMIC INVERSIONS

We have jointly inverted *P* and *SH* waveforms to obtain the focal parameters of the first of the two earthquakes (12:23 UTC). We low-pass filter the seismograms in order to reproduce the response of a long-period (15–100 s) WWSSN instrument. We then invert for the focal parameters using Green's functions

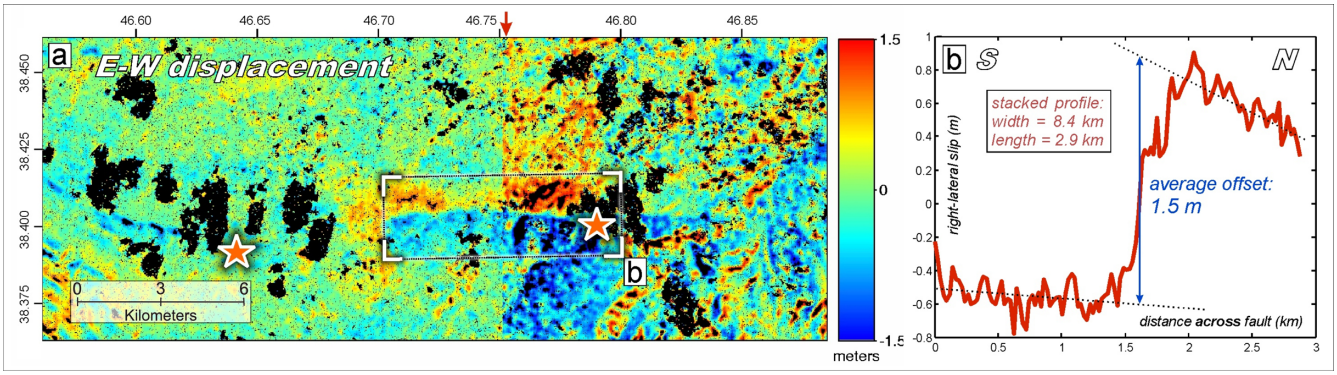

Figure 5. (a) E–W component of horizontal surface motions estimated by cross-correlating WorldView satellite images. The red arrow on the north edge of the map shows the location of the join between two satellite footprints. The red stars show the east and west ends of the surface ruptures mapped in the field. (b) Profile of displacement across the fault from measurements stacked within the white-cornered box in (a).

calculated for a point source, using the MT5 program of Zwick *et al.* (1994) (a version of the algorithm of McCaffrey & Abers 1988; McCaffrey *et al.* 1991). This procedure is commonly used, and thorough descriptions can be found in Nabelek (1984) and Taymaz *et al.* (1991).

Our preferred solution is shown in Fig. 6. The faulting was dominantly strike-slip, and either right-lateral motion on an E–W plane or left-lateral slip on a N–S plane. The seismic inversions constrain the centroid depth to be less than 10 km (with a best fit at 7 km), and the potential error in the strikes of the nodal planes is around 15°. The rake is well-enough constrained to conclude that the motion was dominantly strike-slip.

We were unable to perform a similar inversion for the second (12:34) event. This is because we use data from stations within a distance range of 30°–85°, in order to avoid complications to the waveforms resulting from reverberations in the lithosphere or interactions with the core or core phases (e.g. *SKS*). Within this distance range, the *SH* waves from the 12:34 event were arriving at the same time as surface waves from the 12:23 event, which swamped the body waves from the second event. Although visible, the *P* waves are noisy because of other phases from the first event. However, all of the *P*-wave first motions we can reliably identify were compressional, in agreement with the oblique-thrusting mechanism of the global centroid moment tensor (CMT) solution (shown on Fig. 1) and the US Geological Survey (USGS) W-Phase solution. In addition, the length of the visible *P* waveforms implies an upper-crustal centroid depth (e.g. <20 km), once more in agreement with the global CMT and USGS W-Phase solutions.

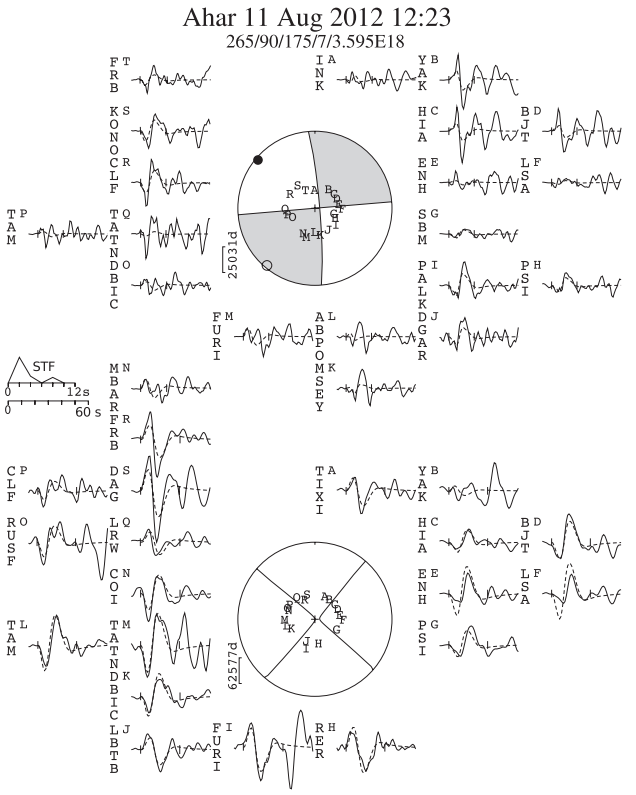

Figure 6. Mechanism of the 12:23 event, from the inversion of *P* and *SH* body waves. The event header shows the strike, dip, rake, centroid depth and scalar seismic moment (in Nm) of the minimum misfit solution. The top focal sphere shows the lower hemisphere stereographic projection of the *P* waveform nodal planes, and the positions of the seismic stations used in the modelling routine. The lower focal sphere shows the *SH* nodal planes. Capital letters next to the station codes correspond to the position on the focal sphere. These are ordered clockwise by azimuth, starting at north. The solid lines are the observed waveforms, and the dashed lines are the synthetics. The inversion window is marked by vertical lines on each waveform. The source time function (STF) is shown, along with the timescale for the waveforms. The amplitude scales for the waveforms are shown below each focal sphere. The *P*- and *T*-axes within the *P* waveform focal sphere are shown by a solid and an open circle, respectively.

5 DISCUSSION

5.1 Locations and slip of the Ahar earthquakes

Field observations show that one of the 2012 August 11 twin Ahar earthquakes ruptured to the surface on an ~E–W striking fault plane, with mostly right-lateral strike-slip motion, close to the crest of a broad topographic ridge. [A ridge top strike-slip fault was also responsible for the M_w 7.3 1990 Rudbar earthquake in the western Alborz mountains of Iran, marked 'R' on Fig. 1 (Berberian *et al.* 1992; Berberian & Walker 2010).] With the available information, we are not able to state definitively which of the two events caused the observed surface ruptures. The slight up-to-the-south vertical motions may imply formation in the first event, as slip on the E–W nodal plane of the second event would lead to up-to-the-north motion (see focal mechanisms on Fig. 1). However, due to uncertainties regarding the extent to which surface ruptures in shallow sediments accurately reflect the motions at depth, the two events do not have sufficiently different mechanisms to allow the observed ruptures to be ascribed definitively to either earthquake.

Our seismic inversions estimate the moment of the first Ahar event to be 3.6×10^{18} Nm. We will initially examine the implications of this moment assuming that the observed surface ruptures were generated by this first event, and then consider the alternative case in which they were formed by the second earthquake. Although our point-source inversions cannot estimate the depth to the base of slip, we can extrapolate from the centroid depth of 7 km, and the fact that the surface rupture may imply that slip reached the surface in this event, to estimate a depth extent of ∼14 km. If we then assume the commonly observed displacement–length ratio in earthquakes of 5×10^{-5} (Scholz 1982; Scholz *et al.* 1986) applies to this event, we can estimate the fault length and slip predicted from the seismology results to be 13 km and 65 cm (using the relation $M_0 = \mu LDu$, where M_0 is the seismic moment, L and D are the length and downdip width of the fault plane and u is the average slip). These seismological estimates are consistent with the field observations (0.5–1 m of slip on a ∼13-km-long fault) and imply a roughly equidimensional fault surface. The moment of the second event is not sufficiently different to that from the first (30 per cent difference in their respective gCMT moments) to allow us to use this method to suggest which earthquake produced the observed ruptures, because of uncertainties in the depth extent of the slip, the unknown centroid depth of the second event and possible variability in displacement–length ratios. However, these calculations suggest that the ruptures probably formed during only one of the two events, and that the other was either blind, or any surface ruptures it produced were not observed.

Based on our certainty that at least one of the earthquakes ruptured an E–W fault, it is possible to suggest two different tectonic interpretations of the Ahar events. One option is that the ∼E–W nodal planes were the fault planes in both events, that they, therefore, had similar slip vectors (Table 1), and that they represent the same overall motion on faults with slightly different strikes (leading to the slightly different components of dip-slip motion). The other alternative is that one of the earthquakes ruptured the N–S striking nodal plane, in which case the events would have had almost perpendicular slip vectors (Table 1). Such a situation is known from other earthquake sequences (e.g. Superstition Hills, California; Hudnut *et al.* 1989), including in Iran (e.g. South Rigan; Walker *et al.* 2013), but is relatively rare. Our lack of knowledge regarding the geometry of both fault planes limits our ability to distinguish confidently between these alternatives.

A coseismic offset was observed in GPS data from a site in Ahar, and is available on the GEO Geohazards Supersite (http://supersites.earthobservations.org/ahar.php). Because the GPS site is multiple fault-lengths away from the seismological epicentres of the two events and the observed ruptures, the ∼30–50 mm northwards and eastwards displacements cannot be used to distinguish between the different possible spatial configurations of the faulting.

Table 1. Mechanisms and possible slip vector azimuths for the two 2012 August 11 Ahar events. The mechanism of the 12:23 event is taken from our own waveform modelling, and that of the 12:34 event from the global CMT catalogue.

Time	Nodal plane	Strike	Dip	Rake	Slip vector azimuth	Method
12:23	E–W	265	90	175	85	Body waves (this study)
	N–S	355	85	0	175	Body waves (this study)
12:34	E–W	255	63	134	100	gCMT
	N–S	10	50	36	345	gCMT

This situation arises because in the far-field, both of the possible orientations of faulting for each earthquake would result in northwards and eastwards offsets at the GPS site. The observed offset is consistent with the magnitudes of the events and their approximate locations, although the multiple trade-offs between fault location and orientation prevent further information about the faulting being derived from this single piece of data.

5.2 The tectonics of NW Iran

Arabia converges obliquely with Eurasia at the longitude of the Turkish–Iranian Plateau at 15–20 mm yr^{-1} to the NNW (e.g. McClusky *et al.* 2003). This oblique convergence is accommodated by spatially separated WNW–ESE striking right-lateral strike-slip faults in the Turkish–Iranian Plateau, and parallel thrust faults in the Greater Caucasus (e.g. Jackson 1992; McClusky *et al.* 2000; Copley & Jackson 2006). There are several different interpretations of the tectonics of the region to the north and east of Lake Urumiyeh (LU on Fig. 1b), and how its faulting relates to the wider collision zone.

Masson *et al.* (2006) measured surface motions using GPS and concluded that the area north of the North Tabriz Fault (NTF on Fig. 1a) is undergoing NE–SW extension at ∼4–8 mm yr^{-1}. Djamour *et al.* (2011) examined an updated GPS survey with denser station coverage from the same region and reduced the estimated extension rate to ∼1–2 mm yr^{-1}, partly because the increase in GPS sites reduced the importance of a single site in the northern tip of Iran which appears to be affected by non-tectonic motion (Djamour *et al.* 2011). However, both of these estimates relied on assumptions about the geometry of the active faults, and analysed the components of GPS velocities parallel and perpendicular to the strikes of the faults included in their tectonic models (either directly, or by using a conceptual model in which the area is divided into a small number of rigid, fault-bounded blocks). The occurrence of the Ahar earthquakes calls into question such an approach. One of the Ahar events ruptured an E–W plane in a dominantly right-lateral sense. This fault is in a different location from, and has a different strike from, the WNW–ESE striking North Tabriz Fault (Fig. 1), which was assumed by Masson *et al.* (2006) and Djamour *et al.* (2011) to be the only fault in the region. The other Ahar event had either an ∼E–W or ∼N–S striking fault plane. Regardless of which of these nodal planes was the fault plane, the fault must have a strike which is different to the North Tabriz Fault (Fig. 1). Both earthquakes occurred north of the North Tabriz Fault, within the region Djamour *et al.* (2011) treat as a rigid block and Masson *et al.* (2006) suggest is extending.

There are, at present, no focal mechanisms of moderate-to-large earthquakes (e.g. $M_w > 5.5$) that indicate active extension in the region NE of Lake Urumiyeh (LU on Fig. 1). Deep (>50 km) normal-faulting events further north, in the central Caspian sea and beneath the Kura Basin (KB on Fig. 1b), are thought to be related to active or recent subduction of Caspian Sea basement, possibly an isolated remnant of oceanic lithosphere (Jackson *et al.* 2002; Mellors *et al.* 2012). The normal faulting to the west of Lake Urumiyeh (the Serow normal faults; SNF on Fig. 1b) is thought to be related to either the kinematic connection between the Main Recent Fault in the Zagros Mountains and the strike-slip faulting north of Lake Van (LV on Fig. 1b), or to along-strike variations in the Arabia–Eurasia convergence direction (Copley & Jackson 2006). Either way, the Serow normal faulting is spatially distinct from, and has a different strike from, the previously proposed extension in the region NE of Lake Urumiyeh.

Based on the mechanisms of the Ahar events, we think it likely that the region NE of the North Tabriz Fault is characterized by right-lateral strike-slip faulting on ~E–W planes, along with some degree of shortening, the regional importance of which is unclear because of our limited knowledge of the geometry of both of the Ahar fault planes. This interpretation of the tectonics of the region is consistent with the GPS velocities in a 'Central Iran' reference frame shown by Masson *et al.* (2006), which indicate E–W right-lateral shear in the region NE of Lake Urumiyeh. In addition, the 1997 M_w 6.0 Ardebil earthquake (A on Fig. 1; Jackson *et al.* 2002) was either right-lateral strike-slip on an E–W plane or left-lateral slip on a N–S plane. The absence of significant N–S left-lateral shear in GPS data from the region suggests that the earthquake had a similar mechanism to the first Ahar event: right-lateral strike-slip on an E–W plane. These earthquakes highlight that the strike-slip component of the overall Arabia–Eurasia movement is distributed across multiple faults in NW Iran. We emphasize that, while common (e.g. Copley & Jackson 2006; Masson *et al.* 2006; Djamour *et al.* 2011), the practice of drawing profiles through GPS velocity fields perpendicular to faults, or constructing block models using the locations of those faults, may provide misleading estimates of slip sense and rate if active faults with other locations and/or strikes are present.

5.3 Seismic hazard and tectonic models of the continental lithosphere

The presence of spatially distributed (and sometimes unrecognized) faults, such as those that ruptured in the Ahar earthquakes, has considerable implications for how we create tectonic models of the continental lithosphere, and what seismic hazard information can be inferred from existing models. Tectonic models that divide continental deformation zones into a small number of rigid blocks can be seen to reproduce the major features observed in GPS velocity fields. For example, models of the Turkish–Iranian Plateau that include a small number of faults with slip rates in excess of ~5 mm yr^{-1}, such as the North Tabriz Fault, provide fits to the GPS observations that are largely within an imposed tolerance (e.g. ~2 mm yr^{-1}, based on the errors associated with the GPS measurements; e.g. Reilinger *et al.* 2006; Djamour *et al.* 2011). Such models are useful for identifying which faults are dominating the deformation field, and for estimating the slip rates on those rapidly moving faults. However, difficulties arise when studying regions that contain faults with slip rates that are similar to, or less than, the tolerance imposed upon the models and the errors in the GPS measurements (e.g. <2 mm yr^{-1}). In such regions, small discrepancies between GPS velocities and the predictions of tectonic block models, due to unmodelled faults, can be obscured by measurement errors and produce misfits that are below the cut-off level for the models to be considered acceptable. Earthquakes and tectonic geomorphology may still allow the faults to be identified, and if so the deformation can usefully be discussed as the relative motion of fault-bounded blocks. If, however, faults remain unknown because they have not ruptured in the limited historical and instrumental earthquake record, and have weak, absent, or unrecognized geomorphological expressions, GPS data alone will not indicate the presence of slow-moving faults. The faults that ruptured in the Ahar earthquakes were not explicitly included in previous tectonic models of the region that were based on GPS data (Reilinger *et al.* 2006; Djamour *et al.* 2011), because they were unknown and they do not produce large differences between the predictions of those models and the GPS observations, which may simply be a consequence of low slip rates compared to the North Tabriz Fault. However, the absence of the Ahar faults in those models also demonstrates that the GPS-derived block models are liable to underestimate seismic hazard in regions where there are slow-moving faults. A similar situation is seen in central Iran, where a large region which is modelled as a rigid block in analyses of GPS data (e.g. Vernant *et al.* 2004) is cut by faults visible in the geomorphology and slipping at rates greater than 1 mm yr^{-1} (Meyer & Le Dortz 2007; Le Dortz *et al.* 2011). In addition to these kinematic problems, any dynamic models constructed to study the stress state and rheology of such a region, which are then compared with the kinematic results of tectonic block models, run the risk of comparing model outputs to an inaccurate representation of the true surface strain-rate field.

The difficulties of characterizing slow-moving faults using GPS velocity fields can be seen in other regions, in addition to Iran. For example, models that use GPS data to divide Greece into small numbers of fault-bounded blocks all identify the Gulf of Corinth, which is opening at ~10 mm yr^{-1}, as a major block-bounding fault system (e.g. Nyst & Thatcher 2004; Reilinger *et al.* 2006), in agreement with the results of earthquake and geomorphological studies (e.g. Armijo *et al.* 1996; Goldsworthy *et al.* 2002). However, the adjacent Gulf of Evia in central Greece is a system of active normal faults that can be identified from geomorphology and catalogues of historical earthquakes up to M_s ~6.9 (e.g. Ambraseys & Jackson 1990; Goldsworthy & Jackson 2001), but is extending at a slow enough rate (~1–2 mm yr^{-1}; Walker *et al.* 2010) that its location and geometry are not accurately represented or required in GPS-derived block models (e.g. Nyst & Thatcher 2004; Reilinger *et al.* 2006). This comparison of GPS-derived tectonic block models with observations of earthquakes and geomorphology, in both NW Iran and central Greece therefore highlights that although the block models can accurately identify the slip rates of rapidly moving faults, they are not sensitive to the locations and slip rates of faults moving at rates similar to the tolerance required of the GPS measurements. Such models will inevitably provide an incomplete picture of the seismic hazard in regions of distributed continental deformation.

6 CONCLUSIONS

We have used a range of techniques to study the twin earthquakes that occurred near Ahar in NW Iran on 2012 August 11. One event ruptured an E–W striking fault in a dominantly right-lateral strike-slip sense, and can account for all the known surface ruptures. The orientation of the other fault plane is not known. These earthquakes highlight the spatially distributed strain in NW Iran, and emphasize that regions of the continents that appear rigid (within some tolerance) to presently available geodetic data may be actively deforming. This deformation, which is undetected by geodesy but may be observable in the geomorphology, is important for both the assessment of seismic hazard, and also for the way in which we construct kinematic models of the deformation of the continental lithosphere. We conclude that NW Iran should not be considered a rigid block, and that there is no evidence for active extension in the region NE of Tabriz.

ACKNOWLEDGEMENTS

We thank Bertrand Meyer and one anonymous reviewer for comments on the manuscript. This work forms part of the NERC- and ESRC-funded 'Earthquakes without Frontiers' project. ASTER GDEM is a product of METI and NASA, and was obtained from the USGS EarthExplorer website. Part of this work was conducted

when JH was supported by NSF grant EAR-1147436 during a post-doc position at University of Southern California. The WorldView data used in this study were also provided through this grant.

REFERENCES

Ambraseys, N.N. & Jackson, J.A., 1990. Seismicity and associated strain of central Greece between 1890 and 1988, *Geophys. J. Int.,* **101,** 663–708.

Ambraseys, N.N. & Melville, C.P., 1982. *A History of Persian Earthquakes*. Cambridge University Press.

Armijo, R., Meyer, B., King, G.C.P., Rigo, A. & Papanastassiou, D., 1996. Quaternary evolution of the Corinth Rift and its implications for the Late Cenozoic evolution of the Aegean, *Geophys. J. Int.,* **126,** 11–53.

Ayoub, F., Leprince, S. & Avouac, J.P., 2009. Co-registration and correlation od aerial photographs for ground deformation measurements, *ISPRS J. Photogramm. Remote Sens.,* **64,** 551–560.

Berberian, M. & Walker, R., 2010. The Rudbar M_w 7.3 earthquake of 1990 June 20; seismotectonics, coseismic and geomorphic displacements, and historic earthquakes of the western 'High-Alborz, Iran, *Geophys. J. Int.,* **182,** 1577–1602.

Berberian, M., Qorashi, M., Jackson, J.A., Priestley, K. & Wallace, T., 1992. The Rudbar-Tarom earthquake of 20 June 1990 in NW Persial preliminary field and seismological observations, and its tectonic significance, *Bull. seism. Soc. Am.,* **82,** 1726–1755.

Copley, A. & Jackson, J., 2006. Active tectonics of the Turkish-Iranian plateau, *Tectonics,* **25,** doi:10.1029/2005TC001906.

Djamour, Y., Vernant, P., Nankali, H.R. & Tavakoli, F., 2011. NW Iran-eastern Turkey present-dat kinematics: results from the Iranian permanent GPS network, *Earth planet. Sci. Lett.,* **307,** 27–34.

Elliott, J., Copley, A., Holley, R., Scharer, K. & Parsons, B., 2013. The 2011 M_w 7.1 van (eastern Turkey) earthquake, *J. geophys. Res.,* **118**(4), 1619–1637.

Engdahl, E.R., van der Hilst, R. & Buland, R., 1998. Global teleseismic earthquake relocation with improved travel times and procedures for depth determination, *Bull. seism. Soc. Am.,* **88,** 722–743.

Geological Survey of Iran. 1978, Ahar Quadrangle Map, the Geological Survey of Iran, scale 1:250,000.

Goldsworthy, M. & Jackson, J., 2001. Migration of activity within normal fault systems: examples from the Quaternary of mainland Greece, *J. Struct. Geol.,* **23,** 489–506.

Goldsworthy, M., Jackson, J. & Haines, J., 2002. The continuity of active fault systems in Greece, *Geophys. J. Int.,* **148,** 596–618.

Hessami, K., Pantosti, D., Tabassi, H., Shabanian, E., Abbassi, M.R., Feghhi, K. & Solaymani, S., 2003. Palaeoearthquakes and slip rates of the North Tabriz Fault, NW Iran: preliminary results, *Ann. Geophys.,* **46,** 903–915.

Hollingsworth, J., Leprince, S., Ayoub, F. & Avouac, J.-P., 2012. Deformation during the 1975–1984 Krafla rifting crisis, NE Iceland, measured from historical optical imagery, *J. geophys. Res.,* **117,** doi:10.1029/2012JB009140.

Hudnut, K.W., Seeber, L. & Pacheco, J., 1989. Cross-fault triggering in the November 1987 Superstition Hills earthquake sequence, southern California, *Geophys. Res. Lett.,* **16,** 199–202.

Jackson, J., Priestley, K., Allen, M. & Berberian, M., 2002. Active tectonics of the South Caspian Basin, *Geophys. J. Int.,* **148,** 214–245.

Jackson, J.A., 1992. Partitioning of strike-slip and convergent motion between Eurasia and Arabia in Eastern Turkey and the Caucasus, *J. geophys. Res.,* **97**(9), 12 471–12 479.

Konca, O., Leprince, S., Avouac, J.-P. & Helmberger, D.V., 2010. Rupture process of the 1999 M_w 7.1 Duzce earthquake from joint analysis of SPOT, GPS, InSAR, strong-motion, and teleseismic data: a supershear rupture with variable rupture velocity, *Bull. seism. Soc. Am.,* **100,** 267–288.

Le Dortz, K. *et al.*, 2011. Dating inset terraces and offset fans along the Deshir Fault (Iran) combining cosmogenic and OSL methods, *Geophys. J. Int.,* **185,** 1147–1174.

Leprince, S., Barbot, S., Ayoub, F. & Avouac, J.-P., 2007. Automatic and precise ortho-rectification, coregistration, and subpixel correlation of satellite images, application to ground deformation measurements, *IEEE Trans. Geosci. Remote Sens.,* **45,** 1529–1558.

Leprince, S., Muse, P. & Avouac, J.-P., 2008. In-flight CCD distortion calibration for pushbroom satellites based on subpixel correlation, *IEEE Trans. Geosci. Remote Sens.,* **46,** 2675–2683.

Masson, F., Djamour, Y., Van Gorp, S., Chery, J., Tatar, M., Tavakoli, F., Nankali, H. & Vernant, P., 2006. Extension in NW Iran driven by the motion of the South Caspian Basin, *Earth planet. Sci. Lett.,* **252,** 180–188.

McCaffrey, R. & Abers, G., 1988. Syn3: a program for inversion of teleseismic body waveforms on microcomputers. Air Force Geophysical Laboratory Technical Report AFGL-TR-88-0099, Hanscomb Air Force Base, MA.

McCaffrey, R., Abers, G. & Zwick, P., 1991. Inversion of teleseismic body waves, in *IASPEI Software Library,* Chap. 3, Vol. 3, IASPEI.

McClusky, S. *et al.*, 2000. Global positioning system constraints on plate kinematics and dynamics in the eastern Mediterranean and Caucasus, *J. geophys. Res.,* **105,** 5695–5719.

McClusky, S., Reilinger, R., Mahmoud, S., Ben Sari, D. & Tealeb, A., 2003. GPS constraints on Africa (Nubia) and Arabia plate motions, *Geophys. J. Int.,* **155,** 126–138.

Mellors, R.J., Jackson, J., Myers, S., Gok, R., Priestley, K., Yetirmishli, G., Turkelli, N. & Godoladze, T., 2012. Deep earthquakes beneath the Northern Caucasus: evidence of active or recent subduction in western Asia, *Bull. seism. Soc. Am.,* **102,** 862–866.

Meyer, B. & Le Dortz, K., 2007. Strike-slip kinematics in Central and Eastern Iran: estimating fault slip-rates averaged over the Holocene, *Tectonics,* **26,** doi:10.1029/2006TC002073.

Nabelek, J., 1984. Determination of earthquake source parameters from inversion of bady waves, *PhD thesis,* MIT, Cambridge, MA.

Nyst, M. & Thatcher, W., 2004. New constraints on the active tectonic deformation of the Aegean, *J. geophys. Res.,* **109,** doi:10.1029/2003JB002830.

Reilinger, R. *et al.*, 2006. GPS constraints on continental deformation in the Africa-Arabia-Eurasia continental collision zone and implications for the dynamics of plate interactions, *J. geophys. Res.,* **111**, B05411, doi:10.1029/2005JB004051.

Scholz, C., 1982. Scaling laws for large earthquakes: consequence for physical models, *Bull. seism. Soc. Am.,* **72,** 1–14.

Scholz, C.H., Aviles, C. & Wesnousky, S., 1986. Scaling differences between large intraplate and interplate earthquakes, *Bull. seism. Soc. Am.,* **76,** 65–70.

Taymaz, T., Jackson, J. & McKenzie, D., 1991. Active tectonics of the north and central Aegean Sea, *Geophys. J. Int.,* **106,** 433–490.

Vernant, P.H. *et al.*, 2004. Present-day crustal deformation and plate kinematics in the Middle East constrained by GPS measurements in Iran and northern Oman, *Geophys. J. Int.,* **157,** 381–398.

Walker, R.T., Claisse, S., Telfer, M., Nissen, E., England, P., Bryant, C. & Bailey, R., 2010. Preliminary estimate of Holocene slip rate on active normal faults bounding the southern coast of the Gulf of Evia, central Greece, *Geosphere,* **6,** 583–593.

Walker, R.T. *et al.*, 2013. The 2010-2011 South Rigan (Baluchestan) earthquake sequence and its implications for distributed deformation and earthquake hazard in southeast Iran, *Geophys. J. Int.,* **193,** 349–374.

Zwick, P., McCaffrey, R. & Abers, C., 1994. Mt5 program. In *IASPEI Software Library,* number 4, IASPEI.